Intracellular Lipid Droplet Accumulation Occurs Early Following Viral Infection and Is Required for an Efficient Interferon Response

EA Monson[1], KM Crosse[1], M Duan[2], W Chen[2], RD O'Shea[1], LM Wakim[3], DR Whelan[2], KJ Helbig[1]

[1] School of Life Sciences, La Trobe University, Melbourne, Australia;

[2] La Trobe Institute for Molecular Science, La Trobe University, Melbourne, Australia.

[3] Department of Microbiology and Immunology, University of Melbourne, at Peter Doherty Institute for Infection and Immunity, Melbourne, Australia.

Correspondence to be addressed to:

Assoc. Prof. Karla Helbig

Department of Physiology, Anatomy and Microbiology

La Trobe University

1 Kingsbury Drive, Bundoora, Vic

3083

Email: k.helbig@latrobe.edu.au

Key words: Lipid Droplet, Virus, Interferon, Organelle, Interferon Stimulated Gene.

Summary

Lipid droplets (LDs) are increasingly recognized as critical organelles in signalling events, transient protein sequestration and inter-organelle interactions. However, the role LDs play in antiviral innate immune pathways remains unknown. Here we demonstrate that induction of LDs occurs as early as 2 hours post viral infection, is transient, and returns to basal levels by 72 hours. This phenomenon occurred following viral infections, both *in vitro* and *in vivo*. Virally driven LD induction was type-I interferon (IFN) independent, however, was dependent on EGFR engagement, offering an alternate mechanism of LD induction in comparison to our traditional understanding of their biogenesis. Additionally, LD induction corresponded with enhanced cellular type-I and -III IFN production in infected cells, with enhanced LD accumulation decreasing viral replication of both HSV-1 and Zika virus (ZIKV). Here, we demonstrate for the first time, that LDs play vital roles in facilitating the magnitude of the early antiviral immune response specifically through the enhanced modulation of IFN following viral infection, and control of viral replication. By identifying LDs as a critical signalling organelle, this data represents a paradigm shift in our understanding of the molecular mechanisms which coordinate an effective antiviral response.

Introduction

Lipid droplets (LDs) are storage organelles that can modulate lipid and energy homeostasis, and historically, this was considered their defining role. More recently, LDs have emerged as a dynamic organelle that frequently interact with other organelles and are involved in protein sequestration and transfer between organelles. LDs have also been demonstrated to act as a scaffolding platform to regulate signalling cascades, highlighting their diverse functions [1–4].

The role of LDs in an infection setting has not been well studied, however, it has been demonstrated that LDs accumulate in leukocytes during inflammatory processes, and they are also induced in human macrophages during bacterial infections [2]. Multiple bacterial strains, including Mycobacterium spp., Chlamydia spp., Klebsiella spp. and Staphylococcus spp. are known to upregulate LDs very early following bacterial infection in both primary and cell culture macrophage models, and this has also been seen for a number of bacterial species in rodent macrophage cell lines [5–7]. Interestingly, *Trypanosoma cruzi* infection of macrophages also induces LDs, however, this response takes 6-12 days to occur following infection[8]. Bacterial- induced LD induction in immune cells has been shown to depend on toll-like

receptor engagement, mainly via TLR2 and TLR4, however, the role of LDs in the outcome of bacterial infection remains largely unknown, and the exact mechanisms for controlling LD induction remain elusive [9,10]. It has been suggested in recent work in the zebrafish model that embryos with higher levels of LDs are more protected from bacterial infections [11] and work in the Drosophila embryo has demonstrated that LDs can bind to histones which are released upon detection of intracellular bacterial LPS and act in a bactericidal manner [12].

Interestingly, LD induction has been demonstrated to be a direct result of immune activation of macrophages by IFN-γ in a HIF-1 dependent signalling pathway [13]. *M. tuberculosis* acquires host lipids in the absence of LDs under normal conditions, however, IFN-γ stimulation of macrophages results in redistribution of host lipids into LDs where M. tuberculosis is unable to acquire them [13]. IFN-γ induced LDs have also been shown to enhance expression of genes involved in LD formation and clustering in INS-1β cells. More importantly, pre-treatment of INS-1 β cells with IFN-γ markedly increased PIC-induced expression of antiviral genes (e.g. *Ifnb*, *Mx1*) [14].

Although induction of LDs has been documented to occur mainly in macrophage models, following infection with bacteria, the ability of viral infection of cells to induce the same response remains relatively unexplored. Recently, viral infection of the positive-stranded RNA viruses, Sindbis and dengue virus, was shown to induce LD formation in the cells of mosquito midgut for the first time [15]. This LD induction was mimicked via synthetic activation of the antiviral innate pathways, Toll and IMD, similar to the induction of bacterial-induced LDs. Although it is known that activation of early innate signalling pathways appears to induce LDs in the presence of bacteria, and in the mosquito midgut when virally infected, the mechanisms at play remain unknown, as does the functional outcome of this LD induction. Here we show for the first time that LDs are induced early following both RNA and DNA viral infection and that this induction is transient in nature and facilitates an effective antiviral response.

Results

Lipid droplets are induced early following viral infection

To determine if LD induction following viral infection is a common phenomenon in mammalian cells, we infected cultured cells with viruses from 3 different viral families. HSV-1, influenza and ZIKV all induced upregulation of LDs at 8 hours following infection, as seen via microscopy (Fig. 1 and Supplementary Fig. 1). Influenza infection of THP-1 monocytes with either the virulent PR8 strain or the more attenuated X-31 strain induced a 6.5-fold increase in LD numbers (Fig. 1A). Primary human foetal immortalised astrocytes were assessed for their ability to upregulate LDs when infected with the neurotropic viruses ZIKV and HSV-1. Astrocytes were seen to have a high average basal level of LDs per cell (approximately 15 per cell) (Fig. 1B and 1C), which was significantly increased by 3.9 and 4-fold following infection of these cells with either ZIKV, or HSV-1, respectively (Fig.1B and 1C). *In vivo*, we examined lung sections taken from both mock and influenza A infected C57BL/6 mice. A clear increase in the presence of large LDs was detected near the bronchioles in the Influenza A infected mice, which was absent in the mock infected mice at both 1- and 3-days post infection (Fig. 1D and Supplementary Fig. 1B).

HSV-1, ZIKV and influenza viruses enter their host cell by either plasma membrane fusion or following endocytosis, prior to the release of their genomic material [16,17]. In order to determine if pattern recognition receptor (PRR) detection of nucleic acid alone would drive an induction of LDs in cells, we stimulated these cells with the synthetic viral mimics, dsRNA (poly I:C, known to mimic viral RNA pathogen associated molecular patterns (PAMPs), and activate the RNA sensors RIG-I and TLR3) or dsDNA (poly dA:dT, known to mimic DNA viral PAMPs, and activate cytosolic DNA sensors). As can be seen using confocal microscopy in Fig. 2A, rhodamine labelled dsRNA and dsDNA clearly induced an upregulation of LDs in primary immortalised astrocytes. To determine if this was a common phenomenon across cell types, similar experiments were performed in primary murine foetal astrocytes, THP-1 monocytes/macrophages, HeLa cells and primary murine embryonic fibroblasts (MEFs). Astrocytes were seen to have a high basal level of LDs, with primary foetal murine astrocytes and immortalized human astrocytes having an average of 22 and 18 LDs per cell respectively; this contrasted with the lower levels of LDs seen in other cell types, which ranged from 6 to 9 LDs per cell (Fig. 2B). All cell types stimulated with either of the viral mimics upregulated LDs at 8 hrs (Fig 2B and S2). Stimulation of cells with dsRNA resulted in LD upregulation fold changes ranging from 4.1-fold in the MEFs to 9.5-fold in the THP-1 macrophages (Fig. 2B). Similarly, dsDNA stimulation resulted in a 4.1-fold induction in HeLa cells and, up to a 10.2-fold induction in the THP-1 monocyte cells

(Fig. 2A). This increase was also shown to be independent of whether FCS was in the culture media (Fig. S2).

Although LD numbers increased in all cell types, the average size of LDs did not (Fig. 2C). The average basal size of LDs was consistent across most cell types, with a diameter range of 280-400 nm (Fig. 2C); however, THP-1 macrophages had a starting average basal LD size of 3100 nm, which did not increase following stimulation with either dsRNA or dsDNA. In contrast, all other cell types had an increased average LD size at 8 hours following dsRNA stimulation, ranging from a 2-fold increase in THP-1 monocytes to a 5.3-fold increase in HeLa cells, with similar size increases observed following dsDNA stimulation also (Fig. 2C). The average size of LDs in the primary immortalised astrocytes following stimulation with viral mimics ranged from 760 to 910 nm (Fig. 2C), however as can be seen in Fig. 2D, there was a significant increase in the number of LDs greater than 1000 nm in these cells, and also, a substantial increase in LDs less than 200 nm, which are referred to as nascent LDs [18]. Nascent LDs made up 24% and 23% of the LD population following dsRNA and dsDNA stimulation respectively, in comparison to only 13% in control-treated cells, perhaps indicating that nucleic acid stimulation drives both the generation of new LDs as well as the growth of existing LD populations.

Lipid Droplet accumulation is transient following detection of intracellular nucleic acids and follows a similar time course to interferon mRNA upregulation.

To define the dynamics of LD induction following the detection of nucleic acids in the cells, we set up a time course series to quantify the speed and longevity of this response. LDs were upregulated as early as 2 hours following either dsRNA or dsDNA stimulation (Fig. 3A and 3B), stayed significantly upregulated for 48 hours post-stimulation and, returned to baseline levels by 72 hours. The average LD number per cell increased from approximately 17 to 28-40 LDs per cell at 2 hours post-stimulation, depending on the stimulation type. Interestingly, dsRNA or dsDNA stimulated cells reached a maximum LD induction between 4-8 hours, however, dsRNA stimulated cells showed an initial decrease in LD number at 24hrs and, a subsequent increase at 48hrs, prior to returning to baseline levels at 72 hrs, indicating a biphasic response, which was not seen following stimulation of the cells with dsDNA. Average LD size per cell was also shown to transiently increase over the same time course

(Supplementary Fig. 3). Interestingly, the induction of LDs coincided with the production of type-I and –III IFN mRNAs in the astrocyte cells (Fig. 3C and 3D), where peak IFN mRNA induction was seen at 8 hours post dsDNA stimulation, but at 24 hours after dsRNA stimulation. IFN mRNA levels showed a trend of returning to basal levels after 72 hours.

Increasing cellular LD numbers acts to enhance the type I and III IFN response to viral infection

We have previously demonstrated that loss of cellular LDs impacts the host cell response to viral infection *in vitro* [19]. To determine if the upregulation of LDs following viral infection plays an anti-viral role in the cell, we initially established a LD induction model in the primary immortalised astrocytes. Addition of oleic acid to cells has previously been shown to enhance LDs minutes following treatment in Huh-7 cells [20]. As can be seen in figure 4A and 4B, the addition of 500 μM of oleic acid to astrocytes in cell culture for 16 hours increased the average LD number from approximately 16 to 43 per cell. Furthermore, despite the increase in cellular LD numbers, stimulation of cells with either dsRNA or dsDNA was able to further upregulate cellular LD levels (Fig 4C and S4). Interestingly, LD upregulation was accompanied by significantly enhanced IFN transcription and translation (Fig. 4D, 4E, 4F and 4G). In the presence of oleic acid enhanced LD numbers, a significant increase in IFN mRNA transcription was seen (Fig. 4D and 4E), although, no increase at the protein level (Fig. 4F and 4G). Addition of dsRNA to the cells in the presence of enhanced LDs (oleic acid treated) showed a 2-fold increase in IFN-β and IFN-λ mRNA at 8 hrs, which was accompanied by a 2-fold increase in the mRNA of the interferon stimulated gene, viperin. However, increases in the transcriptional level for these genes were only observed at 24 hours for IFN-λ and viperin (2 and 2.6-fold respectively; Fig. 4D and 4E). Addition of dsDNA to cells with an enhanced LD content did not increase the IFN-β transcriptional response, however, a small but significant increase in IFN-λ and viperin mRNA was observed at both 8 and 24 hours post-stimulation (1.5 and 2-fold respectively at 8 hours, and 2.5 and 2-fold at 24 hours (Fig. 4D and 4E)). In confirmation of the transcriptional upregulation of IFNs, significantly enhanced protein levels could be seen for both IFN-β and IFN-λ following either dsRNA or dsDNA stimulation of primary immortalised astrocytes with oleic acid induced LDs, in comparison to controls (Fig. 4F and 4G). The presence of upregulated LDs

was able to significantly enhance the production of IFN-β and IFN-λ protein by as much as 2.6 and 3.6-fold in the presence of dsRNA and 2.0 and 2.1-fold in the presence of dsDNA. Interestingly, the production of both IFN-β and IFN-λ was much greater following stimulation with dsDNA in comparison to dsRNA in the astrocyte, with IFN-λ being the dominantly expressed IFN species.

Next, we assessed the host antiviral response to viral infection, in the presence of enhanced LDs. LD loaded cells, when challenged with ZIKV demonstrated a 3.5-fold increase in the production of IFN-β mRNA at 24 hours and a small but significant increase of 1.7-fold at 48 hours post-infection when compared with control infected cells (Fig. 5A). IFN-λ followed a similar trend showing a 3.3 and a 2.2-fold increase at 24 and 48 hours respectively (Fig. 5A), and a 5-fold increase in IFN-λ mRNA at just 6 hours post-infection. Interestingly, when looking at the production of a key antiviral signalling and LD resident protein, viperin, cells with enhanced LDs showed a significant increase in mRNA at 6, 24- and 48-hours post ZIKV infection. Cells infected with the dsDNA virus, HSV-1 also showed a similar trend, where the production of mRNA for both IFN-β and IFN-λ as well as viperin were enhanced in cells pre-treated with oleic acid (Fig. 5B). These results correlated well with a reduced viral load of both ZIKV and HSV-1 at 24 hours (6.3-fold and 2.3-fold for ZIKV and HSV-1 respectively) (Fig. 5C and 5D) and at 48 hours post infection (1.4-fold decrease in ZIKV mRNA and a 2.6-fold decrease in HSV-1 (Fig. 5C and 5D)). This reduction in viral load for ZIKV coincided with a significantly enhanced level of both IFN-β and IFN-λ production by the astrocytes with upregulated LDs (Fig. 5E).

Lipid droplets accumulate in response to IFN, despite initial accumulation being type-I IFN independent

Detection of aberrant nucleic acid in cells drives a rapid interferon response [21]. In order to determine if LD induction following the detection of intracellular nucleic acids required the production of IFN, we stimulated Vero cells, which lack the ability to produce IFN due to spontaneous gene deletions [22,23], with both dsRNA and dsDNA. Both LD number and size were significantly upregulated in Vero cells at 8 hours post-stimulation (Fig. 6A, 6B and Supplementary Fig. 5), indicating that this is an IFN independent event. As can be seen in

figure 6C and 6D, LDs were significantly induced by up to 4.5-fold following interferon stimulation. To show this in a more physiologically relevant setting, astrocyte cells were treated with dsRNA and dsDNA and left to produce IFNs for 24 hours, and their conditioned media was removed and placed on untreated astrocyte cells. Conditioned media from cells stimulated with dsRNA was also shown to induce LDs by 6.3-fold, a similar level to that induced by 1000 U/mL of IFN-β (Fig 6E). Interestingly, conditioned media from cells stimulated with dsDNA showed no increase in LD numbers (Fig. 6E), perhaps indicating the presence of an inhibitor of LD induction. To confirm that it was the presence of secreted IFNs in the conditioned media alone, that was driving the production of LDs, we took conditioned media from both dsRNA and dsDNA stimulated astrocytes and Vero cells at 24 hours following stimulation and placed it back onto untreated cells. As the Vero cells lack the ability to secrete type-I IFNs, we expected to see no induction of LDs in cells receiving conditioned culture media from these cells, which we observed (Fig. 6F). The induction of LDs was only driven with the addition of dsRNA conditioned media removed from astrocytes and placed onto both naive astrocytes and Vero cells. Interestingly, the addition of conditioned culture media from Vero cells stimulated with dsDNA onto untreated astrocytes cells showed a 2.7-fold decrease in the average number of LDs per cell relative to control untreated cells (Fig. 6F). Perhaps, further demonstrating the presence of a secreted negative regulator of LD biogenesis following dsDNA stimulation of astrocytes.

LD Induction Following Nucleic Acid detection is EGFR Mediated

Phospholipase A2 (PLA_2) is an enzyme known to be a key player in LD biogenesis, where it catalyses the hydrolysis of glycerophospholipids to release fatty acids from phospholipid membranes which are then sequestered into the ER membrane leading to the maturation and budding off of mature LDs [18]. Astrocyte cells were treated with $AACOCF_3$, a well-described inhibitor of PLA_2, [24] and their ability to induce LDs was assessed. $AACOCF_3$ was able to inhibit LD biogenesis post serum starvation (Fig. S6A and S6B), confirming that natural LD biogenesis in astrocytes requires PLA_2 activation. To assess whether LD induction following recognition of viral mimics also follows a PLA_2 driven mechanism, cells were treated with $AACOCF_3$ prior to stimulation. Inhibition of PLA_2 did not inhibit the induction of virally induced LDs in the primary immortalized astrocyte cells (Fig. 7A and 7B). EGFR engagement has previously been shown to control LD upregulation in colon cancer [25]. To

assess whether EGFR was important in LD biogenesis following viral mimic stimulation, primary immortalized astrocyte cells were treated with AG-1478, a well-described tyrosine kinase inhibitor of EGFR [26] and stimulated with dsRNA and dsDNA to evaluate LD induction. Astrocyte cells treated with AG-1478 demonstrated no induction of LDs after stimulation with dsRNA or dsDNA, however, AG-1478 did not inhibit the induction of LDs following oleic acid treatment, with LDs being induced approximately 5-fold (Fig. 7C and 7D). Similarly, the treatment of MCF-7 cells (known to lack EGFR [27]), also resulted in no upregulation of LDs following stimulation with viral mimics but was able to upregulate LDs in the presence of oleic acid (Supplementary Fig. 7A and 7B). However, the inhibition of EGFR did not alter LD biogenesis post serum starvation (Fig. 7E), indicating that the EGFR receptor is able to mediate the induction of viral mimic driven LDs, but not natural biogenesis of LDs in astrocytes. Further downstream analysis also demonstrated that the EGFR mediated induction of virally driven LDs relies on subsequent PI3K activation in the cell (Fig. S7).

A time course of LD induction in cells treated with AG-1478 demonstrated that at 8 hours, there is no LD induction, confirming that the initial upregulation of LDs following nucleic acid stimulation is dependent on EGFR. However, at 24 hours post-stimulation, there was a 2.5-fold increase in LD numbers in dsRNA stimulated cells, but not in dsDNA stimulated cells (Fig. 7F). At 48 hours post-stimulation, a similar trend was observed with a 4-fold induction in the dsRNA stimulated cells, but again no LD induction in the dsDNA stimulated cells (Fig. 7F). This result may explain the biphasic expression pattern of LDs seen following dsRNA stimulation of astrocytes, but not dsDNA stimulation (Fig. 3B), particularly if the second wave of LD induction is not dependent on EGFR. To assess this, we treated primary immortalised astrocyte cells with AG-1478 to inhibit EGFR and stimulated them with IFN-β and analysed their LD numbers after 16 hours. There was no significant difference in the upregulation of LDs of control cells compared with cells treated with AG-1478 when stimulated with IFN-β indicating EGFR does not play a role in the upregulation of LDs induced with IFN stimulation (Fig. 7G).

Inhibition of EGFR driven LDs impacts IFN production and attenuates viral infection

We next wanted to understand the relationship between viral-induced EGFR driven LD biogenesis and the regulation of IFN mRNA. Primary immortalised astrocytes were pre-

275 treated with AG-1478 prior to being stimulated with dsRNA and dsDNA, and their ability to
276 upregulate IFN mRNA assessed. Both IFN-β, IFN-λ and viperin mRNA levels were
277 significantly downregulated at 8 hrs post nucleic acid treatment, with little change being
278 present at 24 hrs post-stimulation (Supplementary Fig. 8A). However, the results were more
279 pronounced when comparing IFN mRNA induction following both ZIKV and HSV-1
280 infection. Inhibition of EGFR driven LDs did not impact the ability of ZIKV or HSV-1 to
281 enter astrocytes, as evidenced by the comparisons of the 6 hour time points for both viruses
282 (Fig. 8A and 8B); however viral replication was enhanced by as much as 26 and 24-fold at 24
283 hrs post infection, and 2 and 24-fold at 48 hours post-infection with ZIKV and HSV-1
284 respectively. Additionally, heightened viral nucleic acid levels corresponded to significantly
285 lowered mRNA levels of IFN-β at both the 24 and 48 hr time points for ZIKV and HSV-1
286 infection (Fig. 8C and 8D) as well as significantly reduced IFN-λ mRNA levels for ZIKV at
287 both time points, and at 24 hours post-infection following HSV-1 infection. There was no
288 IFN-λ expression observed at 48 hrs following HSV-1 infection. The production of both type
289 I and III IFN mRNA levels also corresponded to the production of mRNA levels for the
290 interferon stimulated gene viperin, with significantly lowered mRNA levels seen in cells
291 treated with the EGFR inhibitor prior to viral infection. These results are indicative of a
292 reduced ability of the cell to produce IFN following viral infection when LD induction is
293 inhibited using the EGFR kinase inhibitor, AG-1478.

294

295 # Discussion

296 Lipid droplets are well known for their capacity as lipid storage organelles, however, more
297 recently, they have emerged as critical organelles involved in numerous other biological
298 functions. LD biology is an emerging field, with recent discoveries describing roles for LDs
299 in multiple signalling and metabolic pathways as well as protein-protein and inter-organelle
300 interactions [1,3,4]. LDs are now considered an extremely dynamic organelle involved in
301 facilitating multiple cellular pathways and responses, however, their role in immunity
302 remains relatively unexplored. We have previously shown that loss of LD mass impairs the
303 antiviral response, and enhances viral replication [19], however, the dynamic induction of LDs
304 and the mechanism responsible for this, as well as their role in the innate immune signalling
305 response, has not previously been characterised.

It has previously been described that the accumulation of LDs can occur in leukocytes during inflammatory processes, and that LDs are induced by a number of bacterial infections in macrophages (reviewed in [2]). The mechanisms behind such induction have been shown to be dependent on toll-like receptor engagement, however, their role in the outcome of bacterial infection is not known, and the exact mechanisms required for their induction remains elusive [2]. Recently, a role for LDs in the antiviral response was proposed for the mosquito, when viral infection was shown to induce LD formation in the cells of the midgut [15]. As this is a phenomenon that has never been observed in mammalian biology, we sought to understand how and why LDs were induced following viral infection.

We analysed the dynamic induction of LDs post activation of innate signalling pathways in a number of cell types, both primary and non-primary, to assess their ability to induce LDs upon infection. LDs were induced upon infection with ZIKV, influenza or herpes simplex virus-1 (Fig. 1A, B & C) in an *in vitro* setting, as well as early *in vivo* following influenza infection in a murine model (Fig. 1D). Interestingly, members of the Flaviviridae family of viruses (HCV, ZIKV and dengue) have previously been demonstrated to deplete LDs by utilising fatty acids to facilitate aspects of their viral life cycle [28,29], with HCV and Dengue also utilising LDs as a platform for viral assembly, where they induce their lipolysis, and manipulate their biogenesis (reviewed in [30]). Recently, Laufman *et al* (2019) also demonstrated a relationship for enteroviruses with LDs, where replication complexes were shown to tether to LDs via viral proteins, to subvert the host lipolysis machinery, enabling the transfer of fatty acids from LDs and leading to the depletion of LDs in infected cells [31]. Interestingly, these studies were predominantly performed at late time points post viral infection *in vitro*, when viral replication is established. We were able to show a significant upregulation of LDs in primary astrocytes infected with ZIKV (a member of the *Flaviviridae* virus family) at 8 hours post-infection, but could also see an observable down regulation of LDs at 2-3 days post infection of the virus (Supplementary Fig. 9), indicating that it is not a cell type specific response, but rather a function of viral replication at later time points. To better examine the induction of LDs in the absence of viral antagonism of the early innate immune response, we analysed LD dynamics in response to synthetic dsRNA and dsDNA viral mimics (Fig. 3) where it was clearly observed that these PAMPs were able to elicit a rapid upregulation of LDs as early as 2 hours post transfection, which peaked at around 8 hours, and returned to baseline by 72 hours post stimulation. This in part corresponds to what Barletta *et al* (2016) demonstrated in their mosquito model, where LD accumulation was

mimicked via synthetic activation of the Toll and IMD antiviral innate pathways, [15] leading to the hypothesis that the accumulation of LDs may be an important antiviral response in the mosquito. It is interesting to note, that the number, size and composition of LDs vary greatly within cells in a homogenous population as well as in different cell types [32] and although all 5 cell types examined in this study were able to induce LDs upon activation of these pathways, the degree in which they could achieve this differed (Fig. 2B). Furthermore, the average size of LDs in different cell types was also shown to increase with the exception of LDs from THP-1 macrophages (A cell type that already displays a large average size of LDs without prior stimulation), perhaps demonstrating that there is an optimal size range for LDs in respect to their functional importance following a viral infection.

Astrocytes are well known for their fast type I interferon response which can be protective from *flavivirus* infection and virus-induced cytopathic effects [33,34]. Astrocytes also have a very robust type-III IFN response which contributes to their ability to be refractory to HSV-1 infection [35,36]. We were able to demonstrate that LD induction correlated with the production of both type I and III IFN, and that when impeded it significantly impacted the transcriptional IFN response in these cells. Additionally, when cellular LD numbers were enhanced *in vitro*, cells produced significantly higher secreted levels of both type I and III IFNs, which coincided with a significant drop in viral load in the infected cells. Together this suggests that the initial production of LDs following viral infection may play a significant role in limiting early viral replication, perhaps through an enhanced antiviral state in the cell. Interestingly, we were also able to demonstrate that dsRNA, and not dsDNA driven LDs were induced in a bi-phasic manner (Fig. 3), with the second wave likely being induced in an autocrine or paracrine manner following IFN secretion.

LDs are known to be induced via multiple mechanisms, with common LD biogenesis involving the accumulation of neutral lipids (most commonly TAG and sterol esters) between the bilayers of the ER membrane, leading to the budding off of nascent LDs into the cytoplasm [37,38]. Several proteins are involved in LD biogenesis in mammalian cells, including PLA_2, perilipins (PLINs), triacylglycerol (TAG) biosynthetic enzymes, fat-inducing transmembrane proteins (FIT1 and FIT2), SEIPIN and fat-specific storage protein 27 (FSP27) [39] as well as some evidence of additional proteins involved in membrane dynamics (coatomer protein 1, SNAREs, Rabs and atlastin) [40]. Here we demonstrate that virally induced LDs have a different biogenesis mechanism to the normal homeostatic LD biogenesis, and that their

production was driven independently of type-I IFN, however, both type-I and -III IFNs were able to stimulate the induction of LDs in astrocyte cells (fig. 6). There have been previous reports of Type- II IFNs (IFN-γ) inducing LDs during a Mycobacterium infection [13], however, to our knowledge there have been no reports of other interferon species activating LD upregulation. Interestingly, we found that both EGFR and PI3K, but not PLA_2, were driving the induction of LDs following viral infection, however this was not the case for LDs induced by IFNs (Fig. 7, Supplementary Fig. 7). EGFR has also previously been shown to elevate LD numbers in human colon cancer cells [25]. Additionally, increases in LDs were blocked by inhibition of PI3K/mTOR pathways, supporting their dependency on selected upstream pathways. This fits with our findings that EGFR engagement plays a role in the induction of virally induced LDs. As mentioned above, we also observed a bi-phasic induction of LDs following dsRNA stimulation, which was firstly mediated by EGFR, in an interferon independent mechanism, with a second wave of LDs being IFN inducible (fig. 4). It is interesting that this phenomenon was not observed following stimulation of cells with dsDNA, potentially indicating slightly different biogenesis pathways, or alternately the co-induction of a negative regulator of LD biogenesis. Previous seemingly contradictory work has identified both an inhibitory and stimulatory role for EGFR in type-I IFN production [41 42,43].

We have shown that the upregulation of LDs following a viral stimulus plays an antiviral role in the cell; and our work has demonstrated that this upregulation contributes to a heightened type I and III interferon response *in vitro*. However, the exact mechanisms involved in this heightened antiviral state still remain to be elucidated. One possibility is that the LD is being utilised as a platform for protein sequestration that contributes to an enhanced IFN response. Previous work from our team has extensively described the host protein, viperin as having both broad and specific anti-viral properties, which are largely dependent on its localization to the LD [44–47]. Viperin's presence on the LD has been shown to significantly enhance the production of type I IFN following engagement of dsDNA receptors, as well as the TLR7/9 receptors [47,48]. It is plausible that there may still be undiscovered antiviral effectors that require LD localisation.

There is an expanding appreciation for the roles of lipids in the antiviral response during infection, in particular, how they can contribute to the inhibition of viral infections. Lipids have been shown to play numerous roles in activation and regulation of immune cells such as

T lymphocytes and macrophages [49]. Recently, a mechanism was described for the activation of macrophages through the release of a distinct class of extracellular vesicles, which are loaded with fat derived directly from adipocyte LDs [50]. As well as having a signalling role in activating immune cells, certain species of lipids have been shown to modulate immune responses. Polyunsaturated fatty acids (PUFAs) are precursors for the synthesis of numerous bioactive lipid mediators, such as eicosanoids and specialized pro-resolving mediators which are released from various immune cell types to modulate immune responses [51–53] . The PUFA lipid mediator D1 (PD1) has also been demonstrated to inhibit IAV infection in cultured cells [54]. It is also important to note that LD populations both between cells and within a cell are diverse, and can consist of different sizes, numbers and distinct protein or lipid compositions. However, the reason for LD diversity is still unclear [32,55–57]. Lipidomics is a growing field and could be utilised to investigate the role and composition of specific subsets of LDs within cells both prior to, during and following viral infection, to give further insight into whether changes within the lipidome assist in driving an antiviral response. [54]

The early induction of LDs following a viral infection acts to aid the antiviral host response by enhancing the production of interferon. Multiple viruses have been demonstrated to usurp host cell LDs to facilitate their replication cycles, and it is possible that this may also represent a subversion mechanism to disrupt early antiviral signalling, however further work is required to unravel these intersections. LDs are now considered an extremely dynamic organelle involved in the facilitation of multiple cellular pathways and responses, and it is now clear that they are also involved in a pro-host response to viral infection.

Acknowledgements

This work was funded by a La Trobe University Research Focus Area grant, as well as a NHMRC ideas grant (APP1181434) to K.J.H. and D.R.W.. L.W. is funded by an ARC Future Fellowship, D.W. is funded by an ARC DECRA. The authors would like to acknowledge the La Trobe University Microscopy Platform.

Author Contributions

E.A.M. performed the majority of the experiments; M.D. and W.C. assisted in *in vitro* influenza studies, and L.W. performed the murine influenza *in vivo* studies. RO assisted in the isolation of murine astrocytes, and K.M.C. assisted in experiments involving MEFs, K.J.H. was responsible for the overall study design, with E.A.M., D.R.W. and K.M.C. also assisting in experimental direction. K.J.H. and E.A.M. wrote the manuscript; all authors commented on the manuscript.

Declaration of Interests

The authors declare no competing interests

Figure Titles and Legends

Figure 1. Lipid Droplets accumulate in response to IAV, ZIKV and HSV-1 infections

(a) Human THP-1 monocytes were infected with two different strains of influenza- PR8 and X-31 at an MOI 5 and **(b)** Primary immortalised astrocyte cells were infected with either the ZIKV strain MR766 or **(c)** HSV-1 at MOI 5 and stained with Bodipy (409/505) to visualise LDs and DAPI to visualise the cell nuclei. Influenza virus was detected with a αNS2 antibody, ZIKV RNA was detected using an anti-3G1.1 and 2G4 dsRNA antibody and HSV-1 was detected using the anti-HSV-1 antibody ab9533. Greater than 200 cells were analysed in each case using ImageJ analysis software, sourced from two independent biological replicate experiments Bars, 15µm. **(d)** C57BL/6 mice were either mock infected or infected with 10^4 PFU of influenza A virus for 24 or 72 hours prior to removal of both lung lobes for immunofluorescence analysis of LDs via Bodipy staining. Bars, 500µm. (data is represented as mean +/- SEM, n = 200 cells or n = 2 mice. ****=p<0.0001, Student's t-test)

Figure 2. Detection of intracellular dsRNA and dsDNA initiates accumulation of LDs in multiple cell types

(a) Primary immortalised human astrocyte cells stimulated with dsRNA and dsDNA tagged with Rhodamine for 8hrs and stained with Bodipy (409/505) to visualise LDs and DAPI to visualise the cell nuclei. Cells were imaged on a Nikon T*i*E microscope. Original

459 magnification is 60X. Bar, 50μm **(b)** Average number of LDs per cell and **(c)** average LD
460 sizes (diameters) were analysed from greater than 200 cells in a range of cell types, using
461 ImageJ analysis software (n=2 biological replicates). **(d)** LD size distribution in primary
462 immortalised astrocyte cells stimulated with either dsDNA or dsRNA for 8 hours. Bar, 15μm.
463 Data is represented as mean +/- SEM, greater than 300 cells; n=3 biological replicates
464 *=p<0.05, **=p<0.01, ***=p<0.001, ****=p<0.0001, Student's t-test.

465

466 **Figure 3. Lipid Droplet accumulation is transient following detection of intracellular**
467 **nucleic acids**

468 **(a)** Primary immortalised astrocyte cells were stimulated with dsRNA and dsDNA and were
469 fixed at regular time points until 72 hours post stimulation. Cells were stained with Bodipy
470 (409/505) to visualise LDs and DAPI to visualise the cell nuclei. Bar, 50μm **(b)** Average
471 number of LDs per cell were analysed from all time points using ImageJ analysis software.
472 Greater than 200 cells were analysed over 3 separate biological replicates. **(c and d)** Primary
473 immortalised astrocyte cells were stimulated with dsRNA and dsDNA and RTq-PCR was
474 utilised to quantify IFN-β and IFN- λ mRNA up to 72 hours post stimulation. Data is
475 represented as mean +/- SEM, *=p<0.05, **=p<0.01, ***=p<0.001, ****=p<0.0001,
476 Student's t-test.

477 **Figure 4. Increasing cellular LD numbers acts to enhance the type I and III IFN**
478 **response to dsRNA and dsDNA**

479 **(a and b)** Primary immortalised astrocyte cells were treated with 500μM oleic acid for 16
480 hours, prior to stimulation with dsDNA or dsRNA. LDs numbers were assessed with ImageJ
481 analysis software (greater than 200 cells, n=2) Bar, 15μm. **(c)** Primary immortalised astrocyte
482 cells were treated with 500μM oleic acid for 16 hours prior to stimulation with dsDNA or
483 dsRNA and analysed for LD numbers. RT-qPCR was performed to evaluate IFN-β, IFN-λ
484 and viperin mRNA expression at **(d)** 8 hours or **(e)** 24 hrs post stimulation. All results are in
485 comparison to RPLPO expression (n=3). **(f and g)** IFN protein levels in the media from the
486 previous experiments at 16 hours post infection were analysed with ELISA kits for IFN- β
487 and IFN-λ protein. Data is represented as mean +/- SEM, *=p<0.05, **=p<0.01,
488 ***=p<0.001, ****=p<0.0001, Student's t-test for RT-PCRs and 2way multiple comparison
489 ANOVA for ELISA experiments.

Figure 5. Increasing cellular LD numbers enhances IFN responses to restrict ZIKV and HSV-1 viral replication

Primary immortalised astrocyte cells were treated with 500 μM oleic acid for 16 hours prior to infection with **(a)** ZIKV MR766 at MOI 0.1 or **(b)** HSV-1 at MOI 0.01. RT-qPCR was utilised to evaluate IFN-β, IFN-λ and viperin mRNA expression at 8, 24 and 48 hpi. Primary immortalised astrocyte cells were treated with 500 μM oleic acid for 16 hours prior to infection with **(c)** ZIKV at a MOI 0.1 or **(d)** HSV-1 at an MOI 0.01, and RT-qPCR was utilised to evaluate viral replication at 6, 24 and 48 hpi. **(e)** At 16 hours post infection, secreted IFN protein levels from these experiments were analysed with ELISA plates for IFN- β and IFN-λ protein. Data is represented as mean +/- SEM, n=3 biological replicates *=p<0.05, **=p<0.01, ***=p<0.001, ****=p<0.0001, Student's t-test for RT-PCRs and 2way multiple comparison ANOVA for ELISA experiments.

Figure 6. Lipid droplet accumulation following intracellular nucleic acid detection is type I IFN Independent.

(a) Vero cells were stimulated with dsRNA and dsDNA and were stained with Bodipy (409/505) to visualise LDs and DAPI to visualise the cell nuclei at 8 hours post stimulation**.** **(b)** Vero cells were fixed at 8, 24- and 48-hours post stimulation and analysed for LD numbers using ImageJ analysis software (greater than 200 cells (n=2)) Bars, 50μm. **(c)** Primary immortalised astrocyte cells were stimulated with either IFN- β or IFN-λ for 8 hours prior to fixation and staining, and **(d)** LD analysis, all performed as above (greater than 200 cells (n=2)). **(e)** Astrocyte cells were treated with pre-conditioned media from prior dsRNA or dsDNA stimulated astrocyte cells or were stimulated with 1000 U/mL of INF-β and their LD numbers were analysed using ImageJ analysis software (greater than 200 cells (n=2)). **(f)** Astrocyte and Vero cells were treated with dsRNA or dsDNA conditioned media from either astrocytes or Vero cells and their LD numbers were analysed using ImageJ analysis software (greater than 200 cells (n=2)).

Figure 7. LD Induction Following Nucleic Acid detection is EGFR Mediated

Primary immortalised astrocyte cells were treated with 2μM $AACOCF_3$ (PLA_2 inhibitor) for 16 hours prior to stimulation with dsRNA or dsDNA for 8 hours and **(a)** were stained with

Bodipy (409/505) to visualise LDs and DAPI to visualise the cell nuclei at 8 hour post stimulation, and **(b)** average numbers of LDs per cell was analysed using ImageJ analysis software (greater 200 cells, n=2). **(c)** Primary immortalised astrocyte cells were treated with 2μM AG1478 (EGFR inhibitor) 16 hours prior to stimulation with dsRNA or dsDNA, or OA and were stained with Bodipy (409/505) to visualise LDs and DAPI to visualise the cell nuclei, and **(d)** average number of LDs per cell analysed using ImageJ analysis software (greater 200 cells, n=2). **(e)** Primary immortalised astrocyte cells were serum starved for 48 hours, plated into wells and treated with 2 μM AG-14789 or control for 16 hours. All cells were then given fresh full serum media for 36 hours and stained to visualise LDs as above. **(f)** Primary immortalised astrocyte cells were treated with 2μM AG-1478 (EGFR inhibitor) for 16 hours prior to stimulation with dsRNA and dsDNA for up to 72 hours and were fixed at regular time points until 72 hours post stimulation. Average numbers of LDs per cell was analysed using ImageJ analysis software (greater than 200 cells, n=2). **(g)** Primary immortalised astrocyte cells were treated with 2 μM AG-1478 (EGFR inhibitor) for 16 hours prior to stimulation with IFN- β and their LDs were numbers assessed using image J analysis software. Bars, 50μm. Data is represented as mean +/- SEM, *=p<0.05, **=p<0.01, ***=p<0.001, ****=p<0.0001, Student's t-test.

Figure 8. EGFR treatment enhances viral infection and dampens the interferon response to ZIKV and HSV-1

Primary immortalised astrocyte cells were treated with 2 μM AG-1478 (EGFR inhibitor) for 16 hours prior to infection with ZIKV and HSV-1. RT-PCRs were performed to detect viral nucleic acid levels of **(a)** ZIKV and **(b)** HSV-1. RT-qPCR was utilised to evaluate IFN-β, IFN-λ and viperin mRNA expression at 8, 24 and 48 hpi for both **(c)** ZIKV at MOI 0.1 or (D) HSV-1 at MOI 0.01. Data is represented as mean +/- SEM, n=3 biological replicates *=p<0.05, **=p<0.01, ***=p<0.001, ****=p<0.0001, Student's t-test.

Methods

Cells and Culture Conditions

All mammalian cell lines were maintained at 37°C in a 5% CO_2 air atmosphere. Huh-7 human hepatoma cells, HeLa human epithelial cells, HEK293T human embryonic kidney

cells, primary murine embryonic fibroblast (MEF) cells, Vero cells, a green monkey kidney cell line, and Primary Immortalised Astrocytes were all maintained in DMEM (Gibco) containing 10% fetal bovine serum (FBS), 100 units/mL penicillin and 100 μg/mL streptomycin. Human monocytic cells (THP-1) were cultured in high glucose RPMI 1640 medium, supplemented with 10% FBS, 100 units/mL penicillin and 100 μg/mL streptomycin. C6/36 Aedes albopictus cells were maintained in Basal Medium Eagle (BME) supplemented with L-glutamine, MEM non-essential amino acids, sodium pyruvate, 10% FBS and P/S and cultured at 28°C with 5% CO_2. For serum replacement experiments, cells were cultured in serum replacement 3 (sigma, S 2640) in DMEM at a concentration of 10% prior to experiments. All experiments were then performed in serum replacement rather than DMEM+FBS.

Influenza infection of mice

C57BL/6 mice were bred in-house and housed under specific pathogen–free conditions in the animal facility at the Peter Doherty Institute of Infection and Immunity, University of Melbourne, Melbourne, Australia. All experiments were done in accordance with the Institutional Animal Care and Use Committee guidelines of the University of Melbourne. Mice were anesthetized with isoflurane and intranasally infected in a volume of 30 μL with 10^4 plaque forming units (PFU) of mouse adapted influenza A viruses, x31(H3N2) or PR8(H1N1). Mock infected mice received 30 μL of PBS intranasally.

In vitro Viral Infection and Viral Mimics

Monocytes were seeded at 1 x 10^6 per well in 12-well plates and pre-treated into polarisation states 24 hrs prior to infection with Influenza A Virus (IAV). Primary Immortalised Astrocyte cells were seeded at 7 x 10^4 per well in 12-well plates prior to infection with Herpes Simplex Virus-1 (HSV-1) and ZIKV (ZIKV). ZIKV (MR766 strain) and HSV-1 (KOS strain) were diluted in serum-free RPMI at a MOI of 0.1. Cells were washed once with PBS then infected with virus. IAV strains PR8 (H1N1) and X-31 (H3N2) were diluted in serum-free RPMI to a MOI of 1.0. THP-1 monocyte cells were seeded at 1–3 × 10^6 and were co□incubated with either PR8 or X-31 for 1 h in 200 μL AIM medium (RPMI□1640 medium supplemented with HCl to pH 6.0), followed by 8 h in 2 mL complete medium, RPMI□1640 medium supplemented with 10% fetal calf serum, at 37°C containing 5% CO_2.

The viral mimics, poly dA: dT (dsDNA) and poly I: C (dsRNA) (Invivogen) were transfected into cells using PEI transfection reagent (Sigma-Aldrich, MO, USA) as per manufacturer's instructions at a concentration of 1 µg/ml. For interferon stimulations, 1000 U/mL IFN-β (PBL Assays) and 100 ng/mL IFN-λ (IL-29) (R&D Systems) were incubated on cells for 16 h (unless otherwise indicated).

Primary murine astrocyte cultures

The establishment of astrocytic cultures from the brains of C57BL/6 mice (post-natal day 1.5) was performed as described previously [58]. Briefly, forebrains were dissected in ice-cold solution (Hanks balanced salt solution: 137 mM NaCl, 5.37 mM KCl, 4.1 mM $NaHCO_3$, 0.44 mM KH_2PO_4, 0.13 mM Na_2HPO_4, 10 mM HEPES, 1 mM sodium pyruvate, 13 mM d(+)glucose, 0.01 $g \cdot L^{-1}$ phenol red), containing 3 mg·mL−1 BSA and 1.2 mM $MgSO_4$, pH 7.4). Cells were chemically and mechanically dissociated, centrifuged, and the pellet resuspended in astrocytic medium [AM: DMEM, Dulbecco's modified eagle medium, 10% FBS, 100 $U \cdot mL^{-1}$ penicillin/streptomycin, 0.25% (v·V-1) Fungizone], preheated to 36.5°C at a volume of 5 mL per brain and plated at 10 mL per 75 cm^2 flask. Cells were maintained in a humidified incubator supplied with 5% CO^2 at 36.5°C and complete medium changes were carried out twice weekly. When a confluent layer had formed (~10 days *in vitro*), the cells were shaken overnight (180 rpm) and rinsed in fresh medium to remove non-astrocytic cells. Astrocytes were subsequently detached using 5 mM EDTA (10 min at 37°C), plated onto coverslips in 24-well plates at 1×10^4 cells per well, and incubated in a humidified atmosphere at 36.5°C with 5% CO^2 overnight. A full medium change was performed to remove non-adherent cells and medium was subsequently changed every 3–4 days thereafter until cells were ready for use.

Lipid droplet induction and treatments

For enhancing lipid droplets:

Oleic acid (n-9 MUFA, C18:1) - a Long-chain fatty acid was used to increase LDs within cells. OA was purchased from Sigma (Sigma-Aldrich, MO, USA) and dissolved in 0.1% NaOH and 10% bovine serum albumin (BSA). OA was prepared as a 10 mM stock solution and stored at −20°C. BSA was used as a vehicle control. Cells were treated with 500 µM OA in DMEM (+1%BSA) for 16 h.

For Serum Starvation of cells:

Cells were either given low serum media containing 2% FCS, or control serum media containing 10% FCS and were incubated in T75cm^2 flasks for 48 hours prior to plating at the required cell density as previously described [19]. Cell culture media on all experiments was changed 30 minutes prior to the beginning of the experiment, with all transfections and experiments being performed in 10% FCS.

Inhibition of EGFR

Tyrphostin AG1478 (4-(3-chloroanilino-6, 7-dimethoxyquinazoline) mesylate, Mr 411.1) was manufactured by the Institute of Drug Technology (IDT, Melbourne, Australia) and solubilized in DMSO (stock 50 mM). Cells were grown in media containing 2 μM AG1478 or an equivalent amount of vehicle (DMSO, 1:25,000 v/v). In all experiments AG1478 media was discarded, and the cells were washed twice with 1x PBS before being followed in pre-warmed media without AG1478 1 h prior to infection/stimulation.

Inhibition of PLA_2

$AACOCF_3$ (Abcam; ab120350) was utilised to inhibit PLA_2. $AACOCF_3$ was prepared in DMSO and stored at -20□C. Aliquots were diluted in complete DMEM to 2 μM immediately prior to use. The final DMSO concentration was always lower than 0.1% and had no effect on lipid droplet numbers.

Inhibition of PI3K

Wortmannin is a well-described inhibitor of PI3K [59] and was obtained from Sigma, dissolved in DMSO at a concentration of 1 mM. Cells were grown in media containing 100 μM Wortmannin. In all experiments, Wortmannin media was discarded, and the cells were washed twice with PBS before addition of pre-warmed media without Wortmannin 1 h prior to infection/stimulation.

IFN ELISAs

Cell culture supernatant was analysed for IFN-β and IFN-λ release using commercial ELISA kits (Crux Biolab, Human IFN-beta ELISA kit (EK-0041) and RayBiotech inc., Human IL-29 ELISA (ELH-IL29-1)) following the manufacturer's instructions.

640 **Conditioned IFN media experiments**

641 Primary immortalised astrocyte cells or Vero cells were stimulated with dsRNA and dsDNA
642 viral mimics for 4 hours before being washed and replenished with fresh complete DMEM
643 media and left to produce IFNs for a further 12 hours. Media was then taken from these cells,
644 centrifuged to remove any cell debris and placed on freshly seeded unstimulated cells. These
645 cells were left in this conditioned media for 8 hours and fixed with 4% paraformaldehyde
646 (PFA) and their LD numbers were analysed.

647 **Immunofluorescence Microscopy**

648 Bodipy staining for LDs was performed as previously described [19]. For cultured cells, briefly,
649 cells were grown in 24-well plates on 12 mm glass coverslips coated with gelatine (0.2%
650 [v/v]) were washed with PBS, fixed with 4% paraformaldehyde in PBS for 15 min at room
651 temperature and permeabilised with 0.1% Triton X-100 in PBS for 10 min. For staining of
652 LDs, cells were incubated with Bodipy 409/505 1 ng/mL for 1 h and then incubated with
653 DAPI (Sigma-Aldrich, 1 µg/ml) for 5 min at room temperature. Samples were then washed
654 with PBS and mounted with Vectashield Antifade Mounting Medium (Vector Laboratories).
655 Preparation and staining of murine lung frozen sections was done as previously described [60].
656 Briefly, frozen lung sections were prepared by inflating the lungs with optimum cutting
657 temperature (OCT). Frozen sections were cut at 14 µM with a Leica CM 3050 S cryostat and
658 mounted on microscope slides and stored at −80°C. Sections were fixed with 4%
659 paraformaldehyde in PBS for 15 min at room temperature. Sections were then washed with
660 PBS, permeabilised with 0.1% Triton X-100 in PBS for 10 min, washed again and then
661 blocked with 1% BSA for 30 mins. Sections were incubated with 1:1000 αIAV NP for 1
662 hour. Sections were then washed and incubated with Alexa Fluor 555 secondary antibody at
663 1:200 for 1 hour. Bodipy was used to stain for lipid droplets at 1 ng/mL for 1 hour at room
664 temperature, and nuclei were stained with DAPI for 5 minutes at room temperature. Images
665 were then acquired using either a Nikon T*i*E inverted fluorescence microscope or ZEISS
666 confocal microscope. Unless otherwise indicated images were processed using NIS Elements
667 AR v.3.22. (Nikon) and ImageJ analysis software.

668 **Lipid Droplet enumeration**

669 LD numbers and diameters were analysed using quantitative data from the raw ND2 images
670 (from NIS elements) in ImageJ using the particle analysis tool. For each condition, at least 9

fields of view were imaged at 60X magnification from different locations across each coverslip. LDs from at least 100 cells per biological replicate with a minimum of n=2 per experiment being analysed for both LD number and average LD size.

RNA Extraction and Real Time PCR

All experiments involving real-time PCR were performed in 12-well plates with cells seeded at 1×10^6/well (monocytes and macrophages) or 7×10^4/well (all other cell types) 24 hrs prior to infections/stimulations and performed at least in triplicate. Total RNA was extracted from cells using TriSure reagent (Bioline), with first strand cDNA being synthesized from total RNA and reverse transcribed using a Tetro cDNA synthesis kit (Bioline). Quantitative real-time PCR was performed in a CFX Connect Real-Time Detection System (BioRad) to quantitate the relative levels of IFN and interferon stimulated gene mRNA in comparison to the housekeeping gene RPLPO. Primers sequences were as follows: RPLOPO-FP 5'-AGA TGC AGC AGA TCC GCA T-3', RPLPO-RP 5'-GGA TGG CCT TGC GCA-3', IFN-β-FP 5'-AGA AAG GAC GAA CAT TGG GAA A-3', IFN-β-RP 5'-TAG CAG AGC CCT TTT TGA TAA TGT AA-3', IFN-λ -FP 5'-GAA GAG TCA CTC AAG CTG AAA AAC-3', IFN-λ-RP 5'-AGA AGC CTC AGG TCC CAA TTC-3', Viperin-FP 5'GTG AGC AAT GGA AGC CTG ATC-3' , Viperin-RP 5'-GCT GTC ACA GGA GAT AGC GAG AA-3', ZIKV-FP 5'CAG CTG GCA TCA TGA AGA AGA AYC-3', ZIKV-RP 5'CAC YTG TCC CAT CTT YTT CTC C-3', HSV-1 5'-TCG GCG TGG AAG AAA CGA GAG A-3' and HSV-1 5'-CGA ACG CAC CCA AAT CGA CA-3'.

Statistical Analysis

Results are expressed as mean ± SEM. Student's t tests were used for statistical analysis between 2 groups, with $p < 0.05$ considered to be significant. Experiments with 2 or more experimental groups were statistically analysed using an ordinary two-way ANOVA with multiple comparisons. All statistical analysis was performed using Prism 8 (GraphPad Software). All experiments were performed in biological triplicate (unless otherwise stated), and technical duplicates for RT-PCRs.

Supplemental Information titles and legends

Supplementary Figure 1. Influenza, ZIKV and HSV-1 virus infection stimulated the induction of lipid droplets

(a) Human THP-1 monocytes were infected with two different strains of influenza- PR8 and X-31 at MOI 5. Primary immortalised astrocyte cells were infected with either the ZIKV strain MR766 or HSV-1 at MOI 5 and stained with Bodipy (409/505) to visualise lipid droplets and DAPI to visualise the cell nuclei. Influenza virus was detected with a αNS2 antibody, ZIKV RNA was detected using an anti-3G1.1 and 2G4 dsRNA antibody and HSV-1 was detected using the anti-HSV-1 antibody ab9533. Bars, 50μm **(b)** C57BL/6 mice were either mock infected or infected with influenza A virus for either 1 or 3 days prior to removal of both lung lobes for immunofluorescence analysis of lipid droplets via Bodipy staining. Figures represent 3 replicate lung sections. Bars, 50μm

Supplementary Figure 2. Lipid droplets accumulate in multiple cell types in response to detection of dsRNA and dsDNA.

(a) Primary murine astrocyte, HeLa, THP-1 macrophages and MEF cells were stimulated with dsRNA and dsDNA for 8hrs and stained with Bodipy (409/505) to visualise lipid droplets and DAPI to visualise the cell nuclei. Cells were imaged on a Nikon T*i*E microscope. Original magnification is 60X. **(b)** To assess if this induction was dependant on fetal calf serum in the cell media primary immortalised astrocyte cells were grown in serum replacement media, seeded on coverslips and stimulated with dsRNA and dsDNA for 8 hours. Cells were stained with Bodipy (409/505) to visualise lipid droplets and DAPI to visualise the cell nuclei, and average number of lipid droplets per cell analysed using ImageJ analysis software (greater 200 cells, n=2). ****=p<0.0001, Student's t-test. Bars, 50μm.

Supplementary Figure 3. The average size of lipid droplet increases following detection of dsRNA and dsDNA and return to basal sizes at 72 hours.

Primary immortalised astrocyte cells were stimulated with dsRNA and dsDNA and were fixed at regular time points until 72 hours post stimulation. Cells were stained with Bodipy (409/505) to visualise lipid droplets and DAPI to visualise the cell nuclei. **(a)** Average size (diameter) of lipid droplets per cell were analysed from all time points using ImageJ analysis software (greater 200 cells, n=2) *=p<0.05, **=p<0.01, ***=p<0.001, ****=p<0.0001, Student's t-test.

Supplementary Figure 4. Lipid droplets continue to accumulate following dsRNA and dsDNA after oleic acid treatment

Primary immortalised astrocyte cells were treated with 500μM oleic acid for 16 hours, prior to stimulation with dsDNA or dsRNA. **(a)** Lipid droplets numbers were assessed with ImageJ analysis software (greater than 200 cells, n=2). Bars, 50μm

Supplementary Figure 5. The average size of lipid droplet increases following detection of dsRNA and dsDNA in Vero cells

Vero cells were stimulated with dsRNA and dsDNA and were stained with Bodipy (409/505) to visualise lipid droplets and DAPI to visualise the cell nuclei at 8, 24 and 48 hours post stimulation and **(a)** analysed for lipid droplet sizes (diameters) using ImageJ analysis software (greater than 200 cells (n=2)) *=p<0.05, **=p<0.01, ***=p<0.001, ****=p<0.0001, Student's t-test.

Supplementary Figure 6. $AACOCF_3$ treatment inhibits the homeostatic biogenesis of lipid droplets.

(a) Primary immortalised astrocyte cells were treated with 2μM $AACOCF_3$ for 16 hours and LD numbers were compared to control treated cells using ImageJ analysis software (greater than 200 cells (n=2)). **(b)** Primary immortalised astrocyte cells were serum starved for 48 hours, plated into wells and treated with 2μM $AACOCF_3$ (PLA_2 inhibitor) or left as control cells for 16 hours. All cells were then given fresh full serum media for 36 hours and stained with Bodipy (409/505) to visualise lipid droplets and DAPI to visualise the cell nuclei, and average number of lipid droplets per cell analysed using ImageJ analysis software (greater 200 cells, n=2). Bars, 50μm.

Supplementary Figure 7. EGFR and PI3K control the induction of virally induced LDs

(a) MCF-7 cells (known to lack EGFR) were stimulated with dsRNA and dsDNA for 8 hours and visualised for lipid droplet content and **(b)** analysed using ImageJ analysis software (greater than 200 cells (n=2)). **(c)** Primary immortalised astrocyte cells were stimulated with Wortmannin (PI3K inhibitor) and stimulated with dsRNA and dsDNA and their LD numbers were analysed using ImageJ analysis software (greater than 200 cells (n=2)) *=p<0.05, **=p<0.01, ***=p<0.001, ****=p<0.0001, Student's t-test. Bars, 50μm.

Supplementary Figure 8. AG1478 treatment reduces type I and III IFN production in primary immortalised astrocyte cells following dsRNA and dsDNA stimulation

(a) Primary immortalised astrocyte cells were treated with 2μM AG1478 (EGFR inhibitor) for 16 hours prior to stimulation with dsDNA or dsRNA and RT-qPCR was performed to evaluate IFN-β, IFN-λ and viperin mRNA expression at 8 hours and 24 hrs post stimulation.

Supplementary Figure 9. LDs are induced upon initial ZIKV infection, but are downregulated by 48 hours post infection

(a) Primary immortalised astrocyte cells were infected with ZIKV strain MR766 at MOI 5 for up to 72 hours post infection. Cells were stained with Bodipy (409/505) to visualise lipid droplets and DAPI to visualise the cell nuclei, ZIKV RNA was detected using an anti-3G1.1 and 2G4 dsRNA antibody **(b)** the average number of LDs was analysed per cell with ImageJ analysis software (greater 200 cells, n=2) ****=p<0.0001, Student's t-test. Bars, 50μm.

References

1. Arrese, E. L., Saudale, F. Z. & Soulages, J. L. Lipid Droplets as Signaling Platforms Linking Metabolic and Cellular Functions. *Lipid Insights* **7**, 7–16 (2014).
2. den Brok, M. H., Raaijmakers, T. K., Collado-Camps, E. & Adema, G. J. Lipid Droplets as Immune Modulators in Myeloid Cells. *Trends Immunol.* **39**, 380–392 (2018).
3. Gao, Q. & Goodman, J. M. The lipid droplet-a well-connected organelle. *Front Cell Dev Biol* **3**, 49 (2015).
4. Henne, W. M., Reese, M. L. & Goodman, J. M. The assembly of lipid droplets and their roles in challenged cells. *EMBO J.* **38**, (2019).
5. Mattos, K. A. *et al.* Modulation of lipid droplets by Mycobacterium leprae in Schwann cells: a putative mechanism for host lipid acquisition and bacterial survival in phagosomes. *Cell. Microbiol.* **13**, 259–273 (2011).
6. Rank, R. G., Whittimore, J., Bowlin, A. K. & Wyrick, P. B. In vivo ultrastructural analysis of the intimate relationship between polymorphonuclear leukocytes and the chlamydial developmental

cycle. *Infect. Immun.* **79**, 3291–3301 (2011).

7. Nicolaou, G., Goodall, A. H. & Erridge, C. Diverse bacteria promote macrophage foam cell formation via Toll-like receptor-dependent lipid body biosynthesis. *J. Atheroscler. Thromb.* **19**, 137–148 (2012).

8. D'Avila, H. *et al.* Host Cell Lipid Bodies Triggered by Trypanosoma cruzi Infection and Enhanced by the Uptake of Apoptotic Cells Are Associated With Prostaglandin E2 Generation and Increased Parasite Growth. *The Journal of Infectious Diseases* vol. 204 951–961 (2011).

9. Tanigawa, K. *et al.* Expression of adipose differentiation-related protein (ADRP) and perilipin in macrophages infected with Mycobacterium leprae. *FEMS Microbiol. Lett.* **289**, 72–79 (2008).

10. Pacheco, P. *et al.* Lipopolysaccharide-induced leukocyte lipid body formation in vivo: innate immunity elicited intracellular Loci involved in eicosanoid metabolism. *J. Immunol.* **169**, 6498–6506 (2002).

11. Dutta, A., Banerjee, S. & Sinha, D. K. Lipid Droplet metabolism dependent microbial defense in pre-immune zebrafish embryos. *bioRxiv* 478859 (2018) doi:10.1101/478859.

12. Anand, P. *et al.* A novel role for lipid droplets in the organismal antibacterial response. *Elife* **1**, e00003 (2012).

13. Knight, M., Braverman, J., Asfaha, K., Gronert, K. & Stanley, S. Lipid droplet formation in Mycobacterium tuberculosis infected macrophages requires IFN-γ/HIF-1α signaling and supports host defense. *PLoS Pathog.* **14**, e1006874 (2018).

14. Truong, N., Love-Rutledge, S., Lydic, T. & Olson, L. K. Effect of interferon gamma on neutral lipid levels, lipid droplet formation, and antiviral responses in pancreatic islets and INS-1 β cells. *The FASEB Journal* **33**, 654.11–654.11 (2019).

15. Barletta, A. B. F. *et al.* Emerging role of lipid droplets in Aedes aegypti immune response against bacteria and Dengue virus. *Sci. Rep.* **6**, 19928 (2016).

16. Weed, D. J. & Nicola, A. V. Herpes simplex virus Membrane Fusion. *Cell Biology of Herpes Viruses* 29–47 (2017) doi:10.1007/978-3-319-53168-7_2.

17. Cohen, F. S. How Viruses Invade Cells. *Biophysical Journal* vol. 110 1028–1032 (2016).

18. Pol, A., Gross, S. P. & Parton, R. G. Review: biogenesis of the multifunctional lipid droplet:

814 lipids, proteins, and sites. *J. Cell Biol.* **204**, 635–646 (2014).

815 19. Monson, E. A., Crosse, K. M., Das, M. & Helbig, K. J. Lipid droplet density alters the early
816 innate immune response to viral infection. *PLoS One* **13**, e0190597 (2018).

817 20. Rohwedder, A., Zhang, Q., Rudge, S. A. & Wakelam, M. J. O. Lipid droplet formation in
818 response to oleic acid in Huh-7 cells is mediated by the fatty acid receptor FFAR4. *J. Cell Sci.*
819 **127**, 3104–3115 (2014).

820 21. Roers, A., Hiller, B. & Hornung, V. Recognition of Endogenous Nucleic Acids by the Innate
821 Immune System. *Immunity* **44**, 739–754 (2016).

822 22. Desmyter, J., Melnick, J. L. & Rawls, W. E. Defectiveness of interferon production and of
823 rubella virus interference in a line of African green monkey kidney cells (Vero). *J. Virol.* **2**, 955–
824 961 (1968).

825 23. Mosca, J. D. & Pitha, P. M. Transcriptional and posttranscriptional regulation of exogenous
826 human beta interferon gene in simian cells defective in interferon synthesis. *Mol. Cell. Biol.* **6**,
827 2279–2283 (1986).

828 24. Gubern, A. *et al.* Group IVA phospholipase A2 is necessary for the biogenesis of lipid droplets.
829 *J. Biol. Chem.* **283**, 27369–27382 (2008).

830 25. Penrose, H. *et al.* Epidermal growth factor receptor mediated proliferation depends on increased
831 lipid droplet density regulated via a negative regulatory loop with FOXO3/Sirtuin6. *Biochem.*
832 *Biophys. Res. Commun.* **469**, 370–376 (2016).

833 26. Johns, T. G. *et al.* Antitumor efficacy of cytotoxic drugs and the monoclonal antibody 806 is
834 enhanced by the EGF receptor inhibitor AG1478. *Proc. Natl. Acad. Sci. U. S. A.* **100**, 15871–
835 15876 (2003).

836 27. Miller, D. L. *et al.* Emergence of MCF-7 cells overexpressing a transfected epidermal growth
837 factor receptor (EGFR) under estrogen-depleted conditions: evidence for a role of EGFR in
838 breast cancer growth and progression. *Cell Growth Differ.* **5**, 1263–1274 (1994).

839 28. Zhang, J. *et al.* Flaviviruses Exploit the Lipid Droplet Protein AUP1 to Trigger Lipophagy and
840 Drive Virus Production. *Cell Host Microbe* **23**, 819–831.e5 (2018).

841 29. Leier, H. C., Messer, W. B. & Tafesse, F. G. Lipids and pathogenic flaviviruses: An intimate

union. *PLoS Pathog.* **14**, e1006952 (2018).

30. Zhang, J., Lan, Y. & Sanyal, S. Modulation of Lipid Droplet Metabolism-A Potential Target for Therapeutic Intervention in Flaviviridae Infections. *Front. Microbiol.* **8**, 2286 (2017).
31. Laufman, O., Perrino, J. & Andino, R. Viral Generated Inter-Organelle Contacts Redirect Lipid Flux for Genome Replication. *Cell* **178**, 275–289.e16 (2019).
32. Thiam, A. R. & Beller, M. The why, when and how of lipid droplet diversity. *J. Cell Sci.* **130**, 315–324 (2017).
33. Lindqvist, R. *et al.* Fast type I interferon response protects astrocytes from flavivirus infection and virus-induced cytopathic effects. *J. Neuroinflammation* **13**, 277 (2016).
34. Furr, S. R. & Marriott, I. Viral CNS infections: role of glial pattern recognition receptors in neuroinflammation. *Front. Microbiol.* **3**, 201 (2012).
35. Li, J. *et al.* Interferon lambda inhibits herpes simplex virus type I infection of human astrocytes and neurons. *Glia* **59**, 58–67 (2011).
36. Sorgeloos, F., Kreit, M., Hermant, P., Lardinois, C. & Michiels, T. Antiviral type I and type III interferon responses in the central nervous system. *Viruses* **5**, 834–857 (2013).
37. Jackson, C. L. Lipid droplet biogenesis. *Current Opinion in Cell Biology* vol. 59 88–96 (2019).
38. Chapman, K. D., Aziz, M., Dyer, J. M. & Mullen, R. T. Mechanisms of lipid droplet biogenesis. *Biochem. J* **476**, 1929–1942 (2019).
39. Tan, J. S. Y., Seow, C. J. P., Goh, V. J. & Silver, D. L. Recent advances in understanding proteins involved in lipid droplet formation, growth and fusion. *J. Genet. Genomics* **41**, 251–259 (2014).
40. Olzmann, J. A. & Carvalho, P. Dynamics and functions of lipid droplets. *Nat. Rev. Mol. Cell Biol.* **20**, 137–155 (2019).
41. Lupberger, J. *et al.* Epidermal growth factor receptor signaling impairs the antiviral activity of interferon-alpha. *Hepatology* **58**, 1225–1235 (2013).
42. Ueki, I. F., Min-Oo, G. & Kalinowski, A. Respiratory virus–induced EGFR activation suppresses IRF1-dependent interferon λ and antiviral defense in airway epithelium. *Journal of* (2013).
43. Lulli, D., Carbone, M. L. & Pastore, S. Epidermal growth factor receptor inhibitors trigger a type

I interferon response in human skin. *Oncotarget* **7**, 47777–47793 (2016).

44. Helbig, K. J. & Beard, M. R. The role of viperin in the innate antiviral response. *J. Mol. Biol.* **426**, 1210–1219 (2014).

45. Helbig, K. J. *et al.* Viperin is induced following dengue virus type-2 (DENV-2) infection and has anti-viral actions requiring the C-terminal end of viperin. *PLoS Negl. Trop. Dis.* **7**, e2178 (2013).

46. Helbig, K. J. *et al.* The antiviral protein viperin inhibits hepatitis C virus replication via interaction with nonstructural protein 5A. *Hepatology* **54**, 1506–1517 (2011).

47. Crosse, K. M. *et al.* Viperin binds STING and enhances the type-I interferon response following dsDNA detection. *bioRxiv* 493098 (2019) doi:10.1101/493098.

48. Saitoh, T. *et al.* Antiviral protein Viperin promotes Toll-like receptor 7- and Toll-like receptor 9-mediated type I interferon production in plasmacytoid dendritic cells. *Immunity* **34**, 352–363 (2011).

49. Hubler, M. J. & Kennedy, A. J. Role of lipids in the metabolism and activation of immune cells. *J. Nutr. Biochem.* **34**, 1–7 (2016).

50. Antonyak, M. A., Lukey, M. J. & Cerione, R. A. Lipid-filled vesicles modulate macrophages. *Science* vol. 363 931–932 (2019).

51. Dennis, E. A. & Norris, P. C. Eicosanoid storm in infection and inflammation. *Nat. Rev. Immunol.* **15**, 511–523 (2015).

52. Serhan, C. N. Pro-resolving lipid mediators are leads for resolution physiology. *Nature* **510**, 92–101 (2014).

53. Jarc, E. & Petan, T. A twist of FATe: Lipid droplets and inflammatory lipid mediators. *Biochimie* (2019) doi:10.1016/j.biochi.2019.11.016.

54. Morita, M. *et al.* The lipid mediator protectin D1 inhibits influenza virus replication and improves severe influenza. *Cell* **153**, 112–125 (2013).

55. Beller, M. *et al.* Characterization of the Drosophila lipid droplet subproteome. *Mol. Cell. Proteomics* **5**, 1082–1094 (2006).

56. Hsieh, K. *et al.* Perilipin family members preferentially sequester to either triacylglycerol-specific or cholesteryl-ester-specific intracellular lipid storage droplets. *J. Cell Sci.* **125**, 4067–

4076 (2012).

57. Martin, S., Driessen, K., Nixon, S. J., Zerial, M. & Parton, R. G. Regulated localization of Rab18 to lipid droplets: effects of lipolytic stimulation and inhibition of lipid droplet catabolism. *J. Biol. Chem.* **280**, 42325–42335 (2005).

58. O'Shea, R. D. *et al.* Effects of lipopolysaccharide on glial phenotype and activity of glutamate transporters: Evidence for delayed up-regulation and redistribution of GLT-1. *Neurochem. Int.* **48**, 604–610 (2006).

59. Hansen, S. H., Olsson, A. & Casanova, J. E. Wortmannin, an inhibitor of phosphoinositide 3-kinase, inhibits transcytosis in polarized epithelial cells. *J. Biol. Chem.* **270**, 28425–28432 (1995).

60. Zhou, X. & Moore, B. B. Lung Section Staining and Microscopy. *Bio Protoc* **7**, (2017).

Figure 1

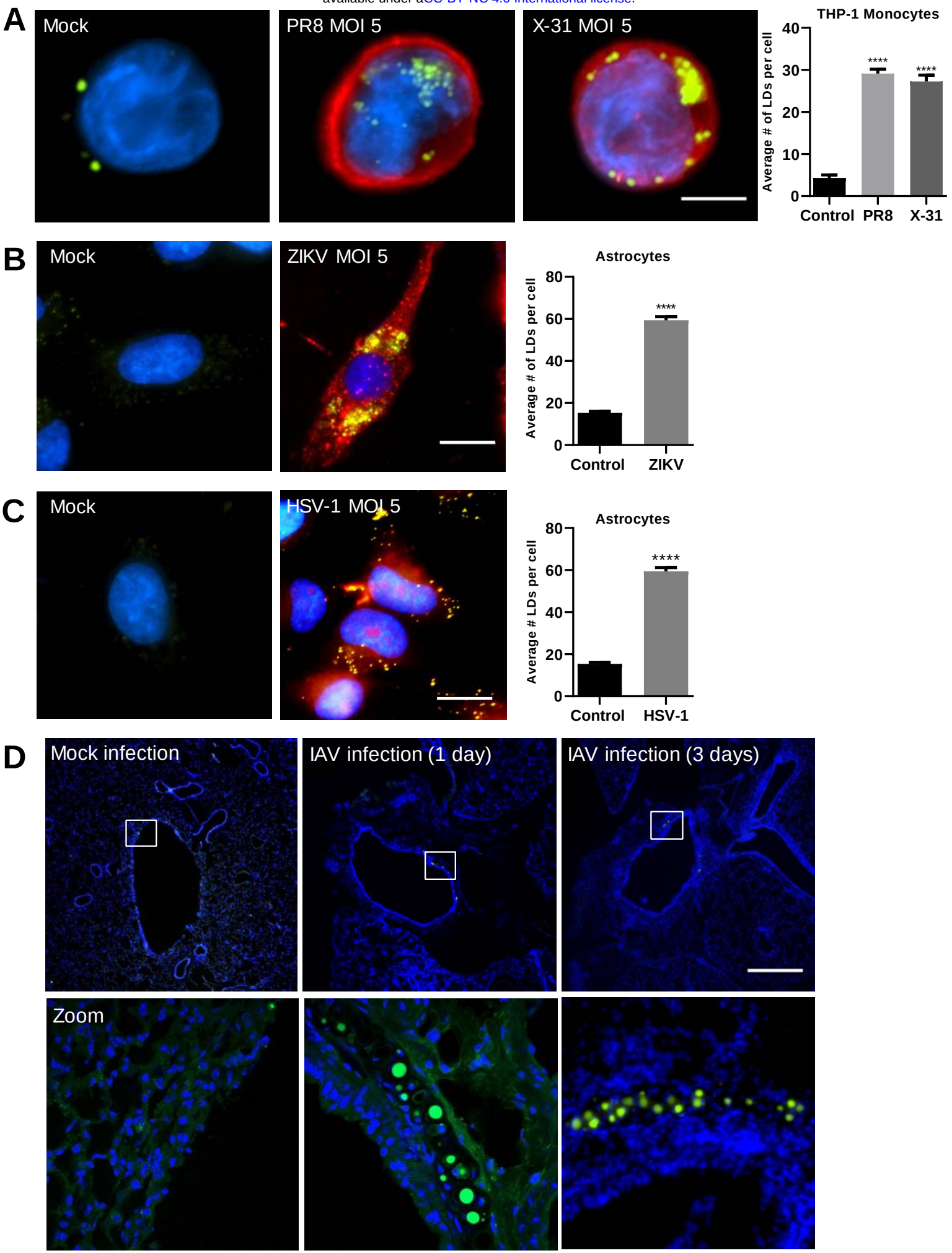

Figure 2

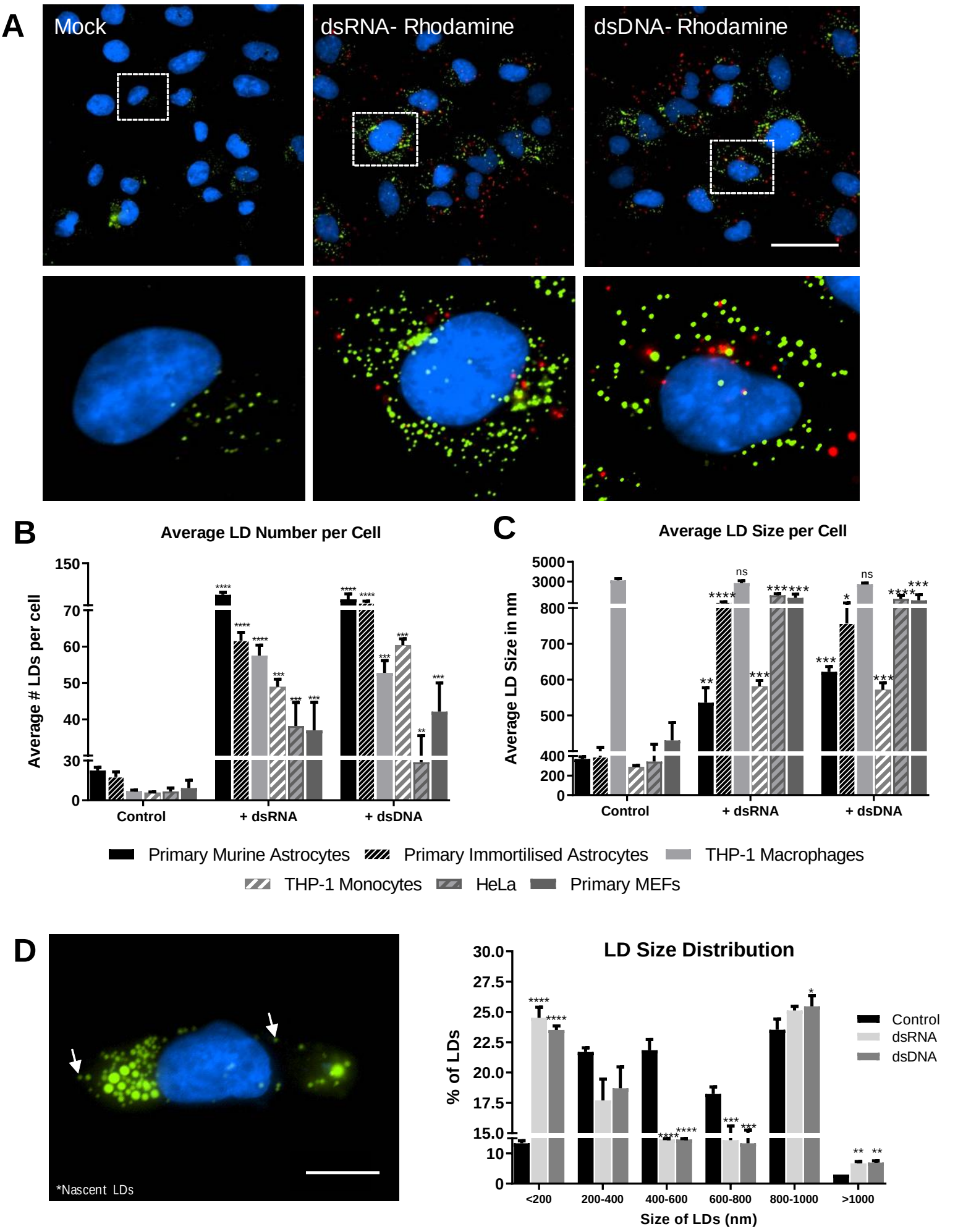

Figure 3

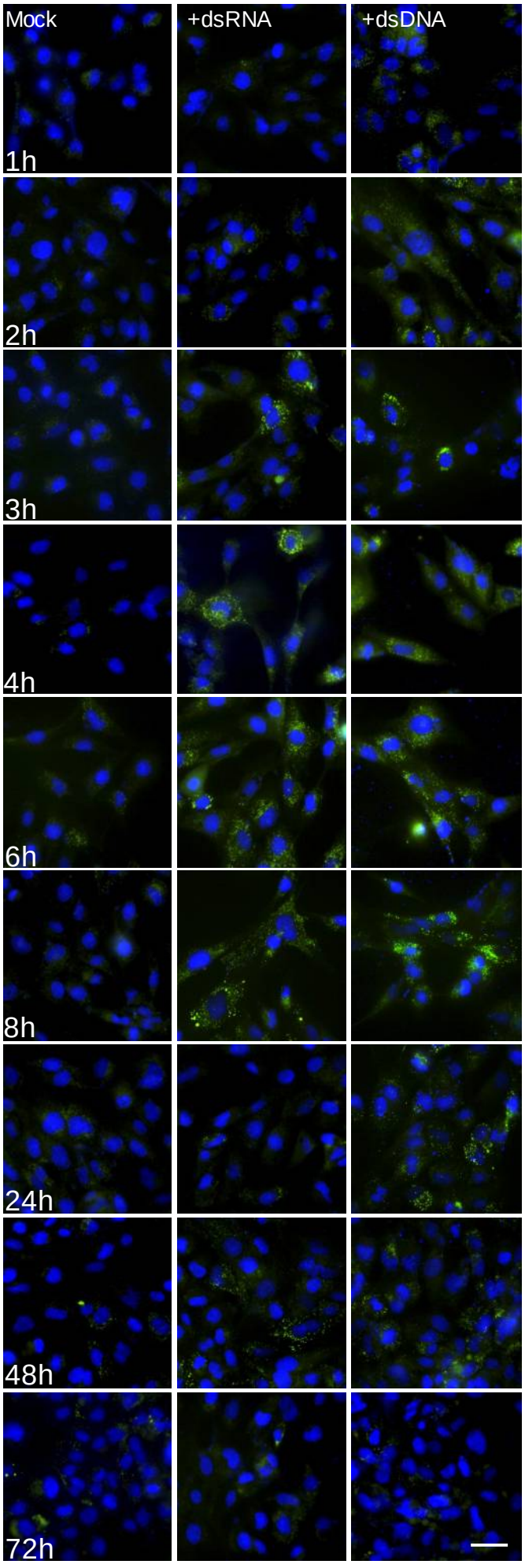

Figure 4

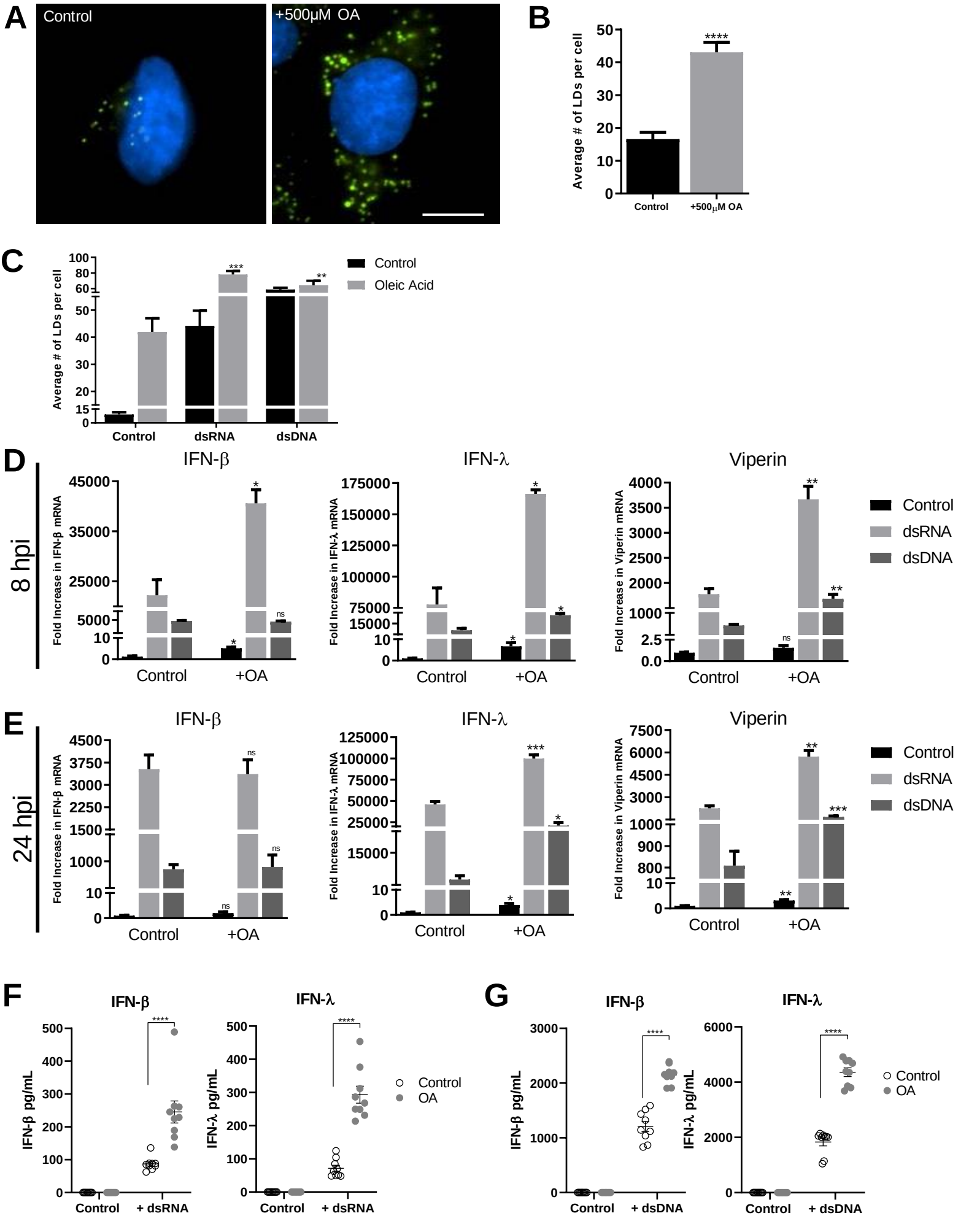

Figure 5

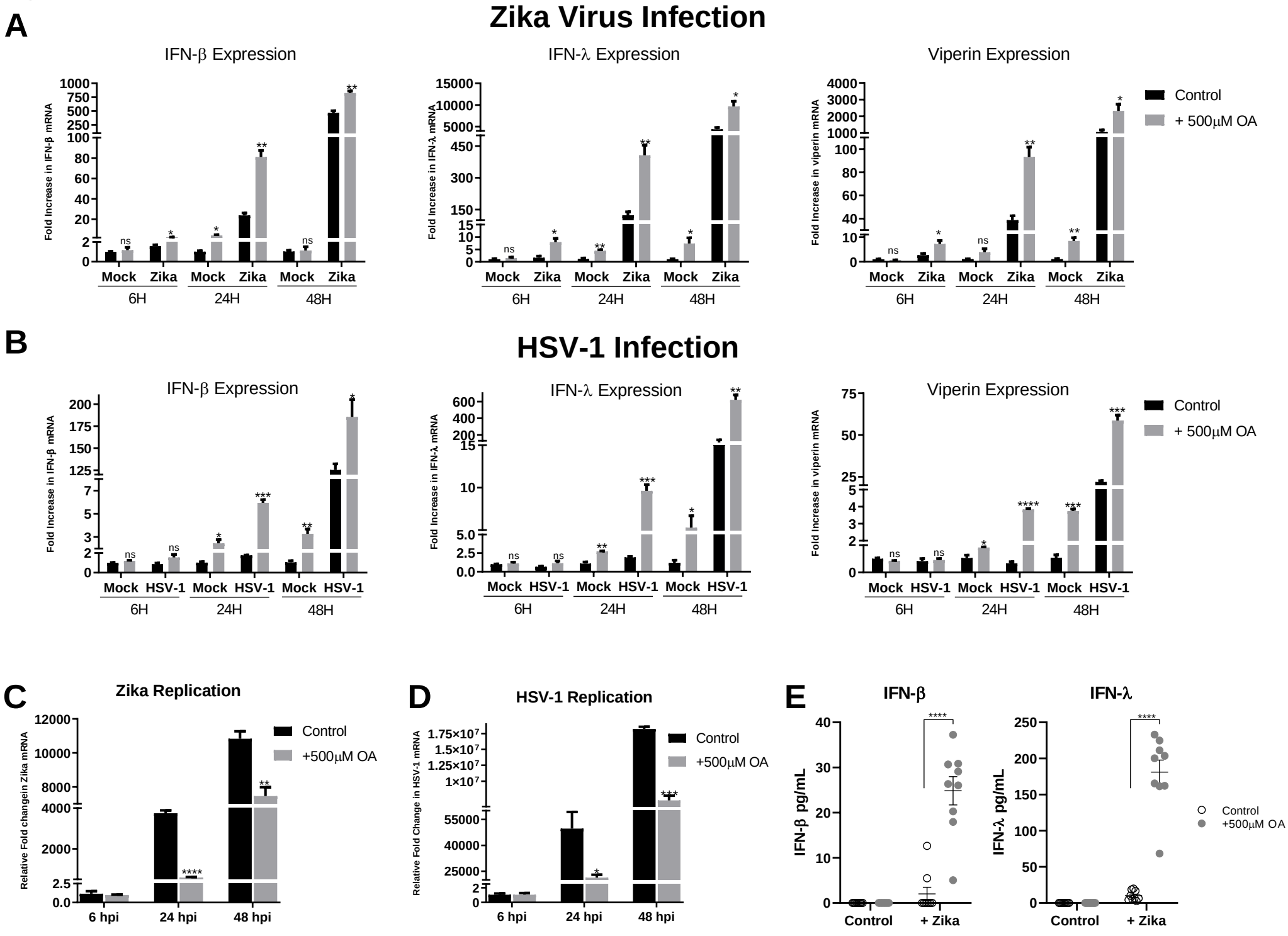
A
Zika Virus Infection
IFN-β Expression
IFN-λ Expression
Viperin Expression
Fold Increase in IFN-β mRNA
Fold Increase in IFN-λ mRNA
Fold Increase in viperin mRNA
Control
+ 500μM OA
Mock
Zika
6H
24H
48H
B
HSV-1 Infection
IFN-β Expression
IFN-λ Expression
Viperin Expression
Mock
HSV-1
C
Zika Replication
Relative Fold changein Zika mRNA
+500μM OA
6 hpi
24 hpi
48 hpi
D
HSV-1 Replication
Relative Fold Change in HSV-1 mRNA
E
IFN-β
IFN-λ
IFN-β pg/mL
IFN-λ pg/mL
Control
+ Zika

Figure 6

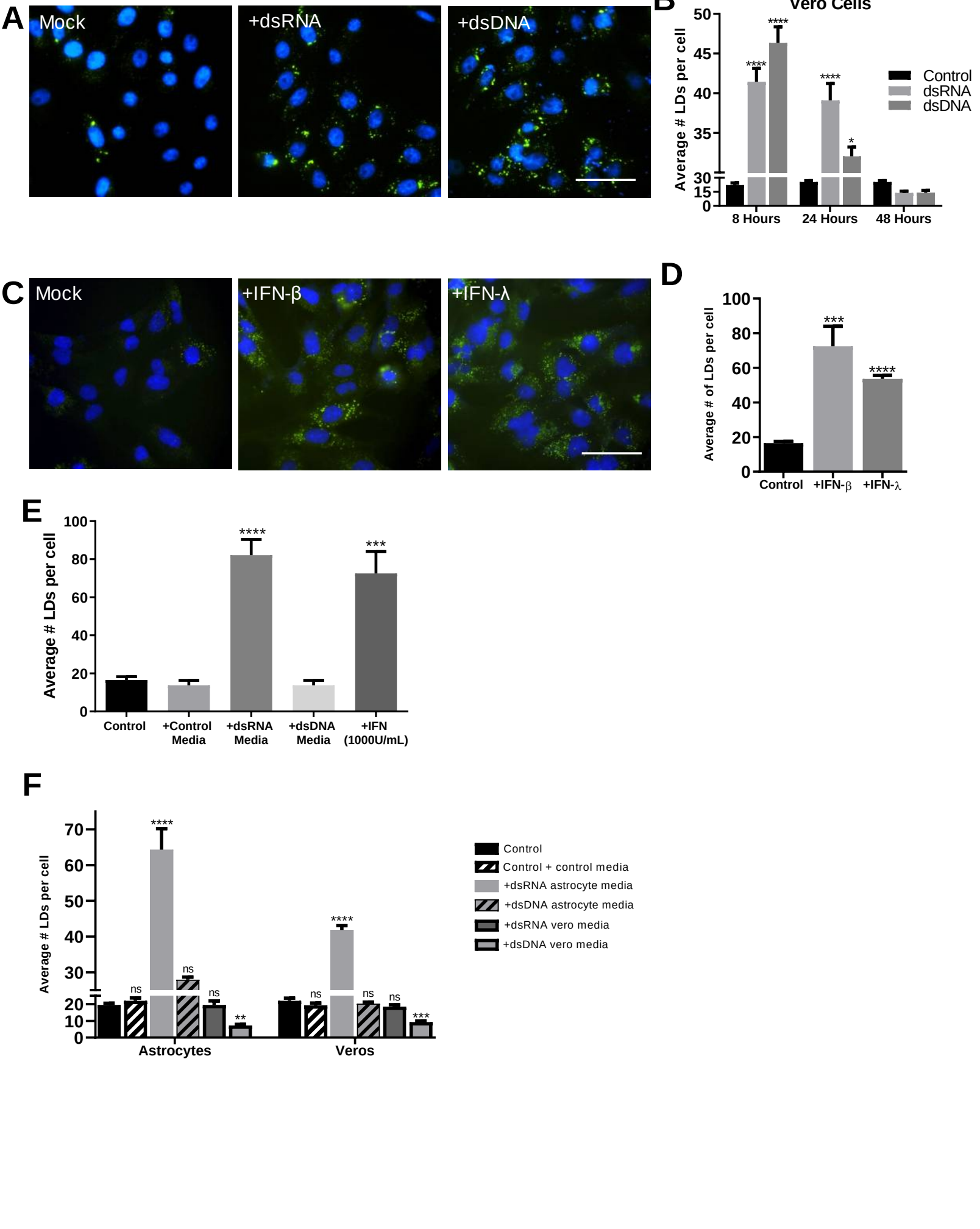

Figure 7

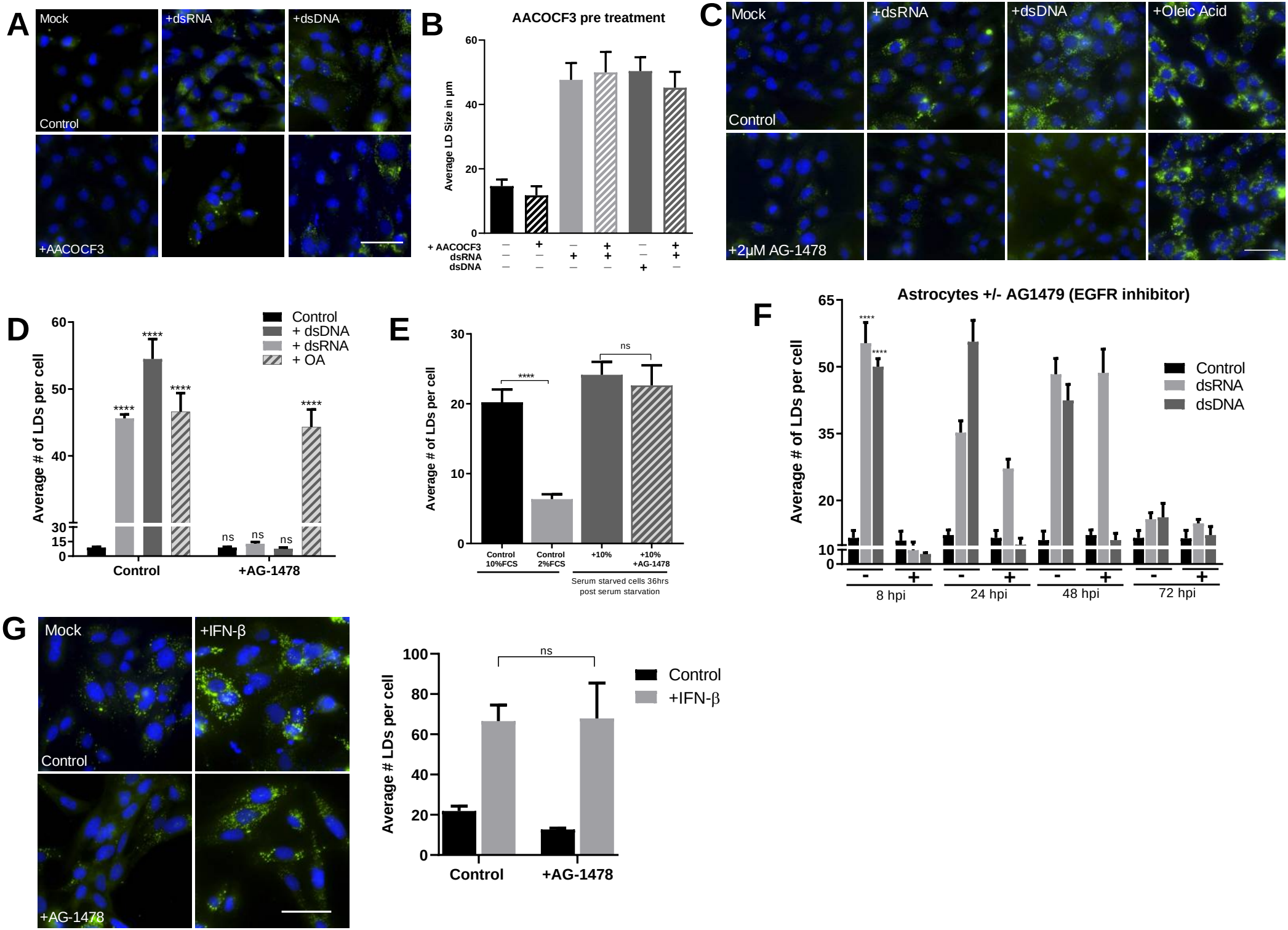
A
Mock
+dsRNA
+dsDNA
Control
+AACOCF3
B
AACOCF3 pre treatment
Average LD Size in µm
60
40
20
0
+ AACOCF3
dsRNA
dsDNA
C
Mock
+dsRNA
+dsDNA
+Oleic Acid
Control
+2µM AG-1478
D
Control
+ dsDNA
+ dsRNA
+ OA
Average # of LDs per cell
60
50
40
30
15
0
****
ns
Control
+AG-1478
E
Average # of LDs per cell
30
20
10
0
****
ns
Control 10%FCS
Control 2%FCS
+10%
+10% +AG-1478
Serum starved cells 36hrs post serum starvation
F
Astrocytes +/- AG1479 (EGFR inhibitor)
Average # of LDs per cell
65
50
35
20
10
0
****
Control
dsRNA
dsDNA
-
+
8 hpi
24 hpi
48 hpi
72 hpi
G
Mock
+IFN-β
Control
+AG-1478
Average # LDs per cell
100
80
60
40
20
0
ns
Control
+IFN-β
Control
+AG-1478

Figure 8

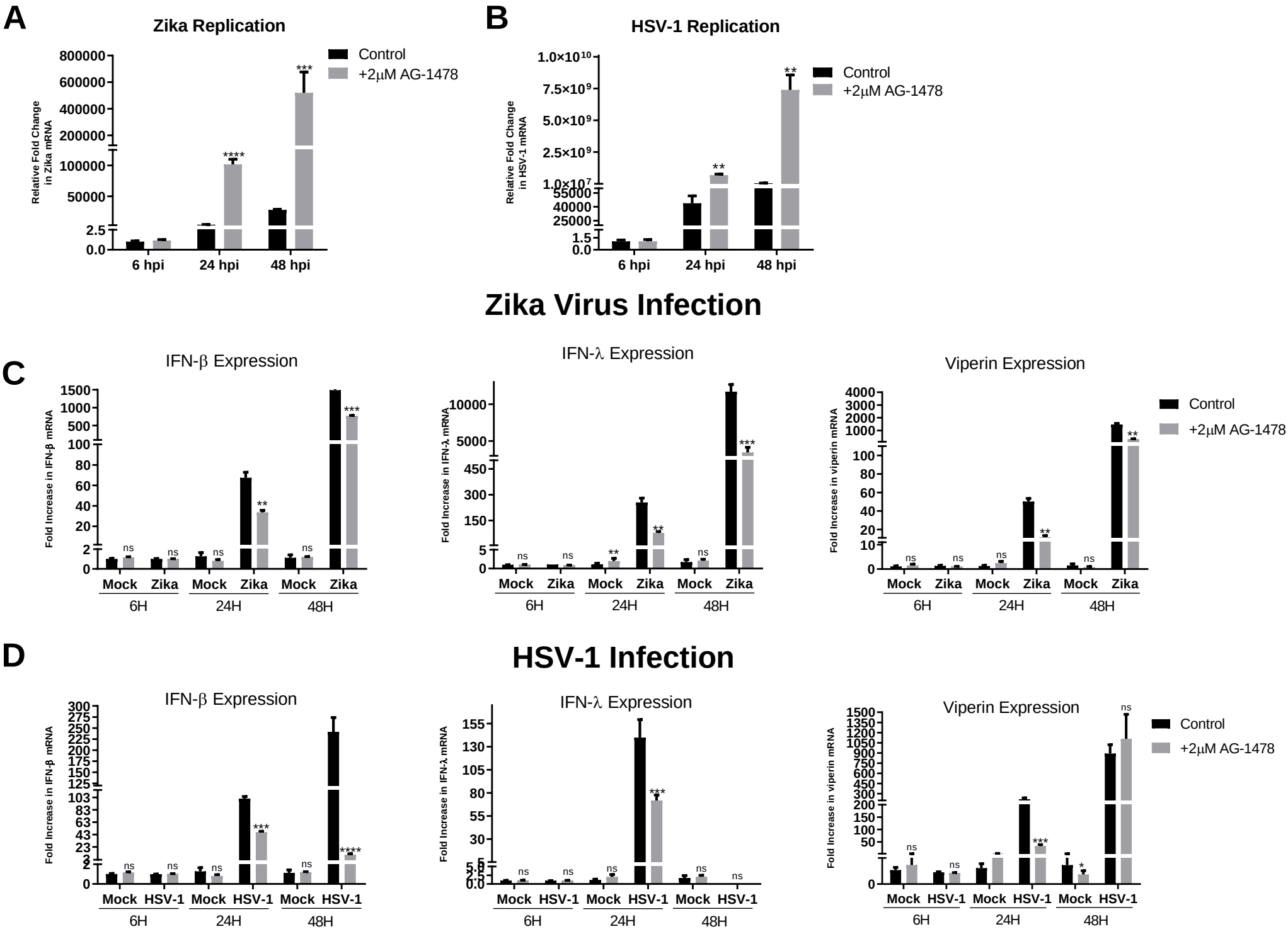
A
Zika Replication
Relative Fold Change in Zika mRNA
Control
+2μM AG-1478
6 hpi
24 hpi
48 hpi
B
HSV-1 Replication
Relative Fold Change in HSV-1 mRNA
Control
+2μM AG-1478
6 hpi
24 hpi
48 hpi
Zika Virus Infection
C
IFN-β Expression
Fold Increase in IFN-β mRNA
IFN-λ Expression
Fold Increase in IFN-λ mRNA
Viperin Expression
Fold Increase in viperin mRNA
Control
+2μM AG-1478
Mock
Zika
6H
24H
48H
HSV-1 Infection
D
IFN-β Expression
Fold Increase in IFN-β mRNA
IFN-λ Expression
Fold Increase in IFN-λ mRNA
Viperin Expression
Fold Increase in viperin mRNA
Control
+2μM AG-1478
Mock
HSV-1
6H
24H
48H